Scale dependence of *in-situ* permeability measurements in the Nankai accretionary prism: The role of fractures

David F. Boutt,[1] Demian Saffer,[2] Mai-Linh Doan,[3] Weiren Lin,[4] Takatoshi Ito,[5] Yasuyuki Kano,[6] Peter Flemings,[7] Lisa C. McNeill,[8] Timothy Byrne,[9] Nicholas W. Hayman,[10] and Kyaw Thu Moe[11]

Received 3 February 2012; revised 5 March 2012; accepted 8 March 2012; published 6 April 2012.

[1] Modeling studies suggest that fluid permeability is an important control on the maintenance and distribution of pore fluid pressures at subduction zones generated through tectonic loading. Yet, to date, few data are available to constrain permeability of these materials, at appropriate scales. During IODP Expedition 319, downhole measurements of permeability within the uppermost accretionary wedge offshore SW Japan were made using a dual-packer device to isolate 1 m sections of borehole at a depth of 1500 m below sea floor. Analyses of pressure transients using numerical models suggest a range of in-situ fluid permeabilities (5E-15–9E-17 m^2). These values are significantly higher than those measured on core samples (2E-19 m^2). Borehole imagery and cores suggests the presence of multiple open fractures at this depth of measurement. These observations suggest that open permeable natural fractures at modest fracture densities could be important contributors to overall prism permeability structure at these scales. **Citation:** Boutt, D. F., et al. (2012), Scale dependence of in-situ permeability measurements in the Nankai accretionary prism: The role of fractures, *Geophys. Res. Lett.*, *39*, L07302, doi:10.1029/2012GL051216.

1. Introduction

[2] Fluids play an important role in the localization, degree, and nature of faulting at subduction zones, through their impact on effective stress [*Bekins et al.*, 1995; *Davis et al.*, 1983; *Scholz*, 1998]. Modeling studies of both accretionary and non-accretionary subduction zones indicate that fluid permeability is an important control on the development and maintenance of excess pore fluid pressures generated through accretion and compaction processes [*Bekins et al.*, 1995; *Bruckmann et al.*, 1997; *Saffer and Bekins*, 1998, 2002; *Gamage and Screaton*, 2006; *Matmon and Bekins*, 2006]. Sediment permeability in these settings can vary by several orders of magnitude due to variations in lithology, compaction state, and diagenetic history [e.g., *Gamage et al.*, 2011], changes in effective stress [*Bekins et al.*, 2011], or the presence of core-scale fractures [*Brown*, 1995]. Most permeability measurements come from core samples of marine sediments; comparatively few in-situ measurements have been conducted [*Davis et al.*, 2000; *Davis and Becker*, 2002; *Becker and Davis*, 2004; *Fisher*, 2005; *Fisher and Zwart*, 1996], and these have focused primarily on fault zones or basaltic oceanic crust using techniques that differ from those presented in this paper. An important question remains about permeabilities at length scales larger than the core scale and how these are impacted by lithologic heterogenity and non-diagenetic processes. In this paper, we present evidence for permeabilities within the interior of an active accretionary wedge that are significantly greater than similar core-scale measurements, possibly due to the presence of open and connected fractures at scales greater than the core scale [*Hsieh*, 1998].

2. Site C0009 and Downhole Measurements

[3] The Nankai Trough Seismogenic Zone Experiment (NanTroSEIZE), a complex scientific drilling project conducted by the Integrated Ocean Drilling Program (IODP), began in 2007 in the Nankai subduction zone, southwest Japan, where $M_w \sim 8$ class great earthquakes repeat at intervals of 100–200 years as a result of the convergence of the Philippine Sea and Eurasian plates (Figure 1). During IODP Expedition 319 D/V Chikyu carried out borehole drilling at Site C0009 within the forearc basin and underlying prism, using riser drilling for the first time in scientific ocean drilling and enabling high quality in situ measurement techniques. A single borehole was drilled at this site, from the seafloor (2054 m water depth) to ~700 mbsf by riserless drilling, and from 700 mbsf to 1600 mbsf by riser drilling. From 0 mbsf to 1285 mbsf, the borehole penetrated Holocene to late Pliocene deposits of the Kumano Basin, characterized by silty mud and mudstones with sand interbeds (lithologic Units I-III). From 1285 mbsf to a total depth of 1600 mbsf, the borehole penetrated shallow to moderately dipping beds of late Miocene silty mudstone with minor silt interbeds (Unit IV). This unit is interpreted as the uppermost interior accretionary wedge, composed of a weakly deformed package of accreted trench sediments [*Saffer et al.*, 2010]. Within Unit IV, cores were recovered from 1509.7 to 1593.9 mbsf. Lithologies within the cored interval include brown-gray silty claystone, minor

[1]Department of Geosciences, University of Massachusetts-Amherst, Amherst, MA, USA.
[2]Department of Geosciences, Pennsylvania State University, University Park, Pennsylvania, USA.
[3]ISTerre, Université Joseph Fourier, Grenoble, France.
[4]Kochi Institute for Core Sample Research, JAMSTEC, Nankoku, Japan.
[5]Institute of Fluid Science, Tohoku University, Sendai, Japan.
[6]Disaster Prevention Research Institute, Kyoto University, Uji, Japan.
[7]Jackson School of Geosciences, University of Texas at Austin, Austin, Texas, USA.
[8]Southampton Oceanography Centre, University of Southampton, Southampton, UK.
[9]Center for Integrative Geosciences, University of Connecticut, Storrs, Connecticut, USA.
[10]Institute for Geophysics, University of Texas at Austin, Austin, Texas, USA.
[11]Center for Deep Earth Exploration, JAMSTEC, Yokohama, Japan.

0094-8276/12/2012GL051216

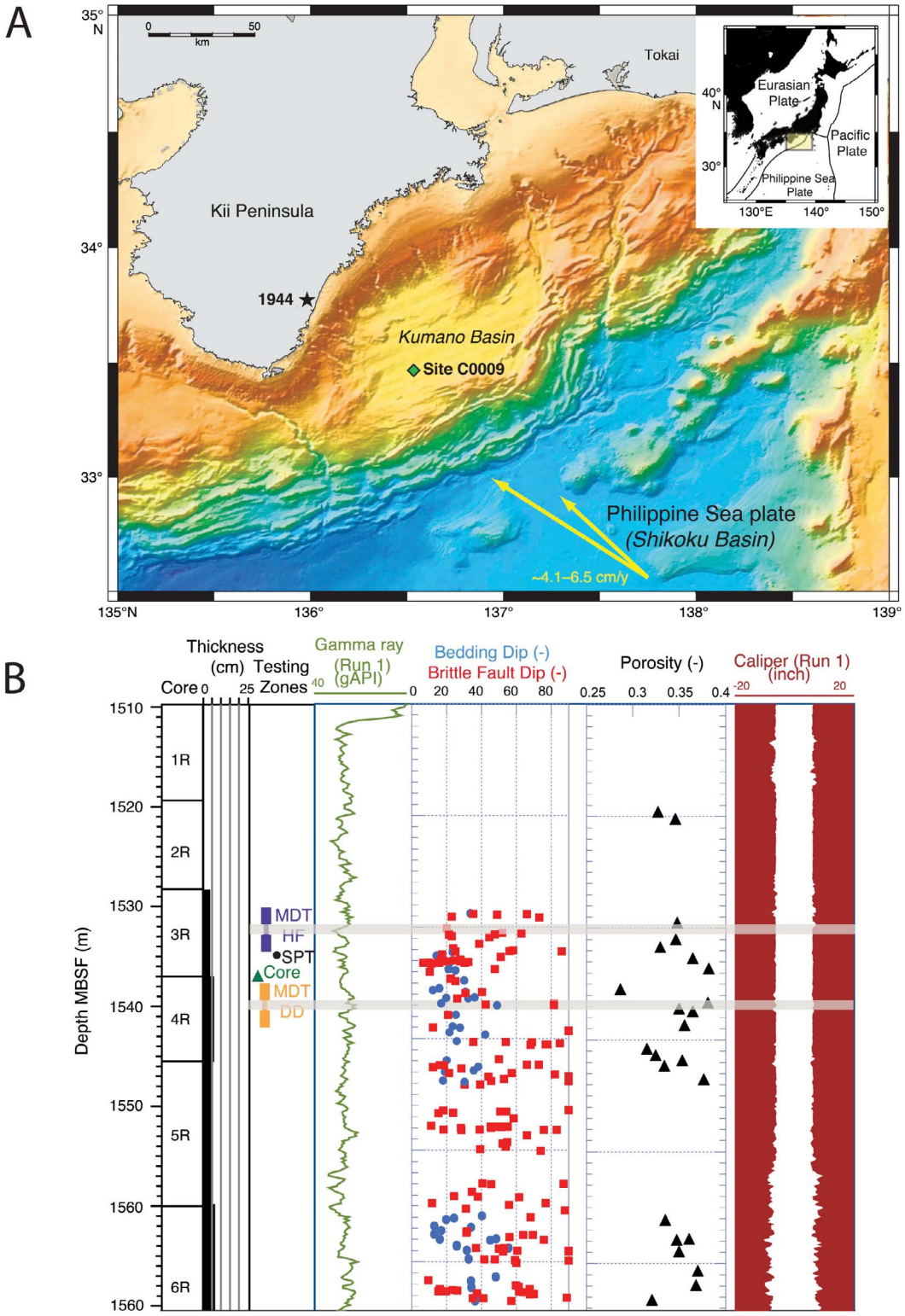

Figure 1. (a) Location of Site C0009 in the Kumano Basin offshore the Kii Peninsula, Japan and location of the NanTroSEIZE drilling project where an accretionary prism is formed by the subduction of the Philippine plate under the Eurasian plate. (b) From left to right location of and number of cores, thickness of sand layers, MST testing zones, gamma ray log, compilation of core-based fracture measurements, core porosity, and caliper log within the cored section of site C0009.

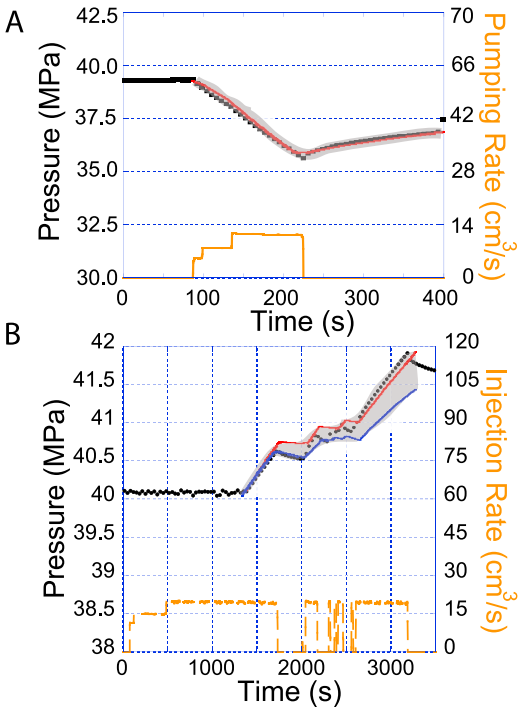

Figure 2. (a) Pore pressure (left axis) and pumping rate (right axis) for the MDT - draw down test at 1539.7 mbsf. Black dots are the observed pore pressure with the test interval and the red solid line is the best fit simulation result. (b) Pore pressure (left axis) and pumping rate (right axis) for the MDT - hydraulic fracture test at 1532.7 mbsf. Black dots are the observed pore pressure within the test interval and the red solid line reflects a permeability of 1.5E-15 m^2 and the blue solid line is 5.5E-15 m^2 which reflect the range in properties used to bracket the data using best fit models.

interbeds of brown-gray siltstone- sandstone, and minor interbeds of light gray fine vitric tuff. Porosity measured on the core samples ranges from 28% to 44%, with an average value of 34%. Within Unit IV, shear zones, natural open fractures and faults, slickenlined faults, and vein structures were identified in the cores (locations are indicated on Figure 1). Active faults are hosted within the interior of the wedge observed both in reflection seismic profiles and recent very low frequency earthquake observations.

2.1. Core-Based Fracture Density Measurements

[4] The distribution and geometry of deformation structures in the retrieved cores from Site C0009 were also characterized by the shipboard party [*Saffer et al.*, 2010], and two dominant structures were recognized: faults and shear zones. Faults are relatively planar zones of deformation often characterized by a single band of concentrated deformation at the scale of the core. Many of the faults also occurred as open fractures in the opened core barrel, often revealing polished or slickensided surfaces. A little over 200 faults were documented in the 60 meters of recovered core, indicating a fault density of about 3.4 faults per meter (Figure 1b). In contrast, the shear zones formed more irregular, wavy bands of deformation that appeared to be healed or annealed as they rarely formed open fractures in the opened core barrel, and when broken along the deformation zone, the slip surface was rough and irregular. The shear zones were also often crosscut by the faults, suggesting that they were older, which is consistent with their annealed character in the open core barrel. A little over 160 shear zones were documented in the 60 m of recovered core, indicating a shear zone density of 2.8 shear zones per meter.

2.2. Logging and Testing

[5] After drilling, we conducted wireline logging runs from ~700 mbsf to 1600 mbsf. Resistivity logs provide evidence of a mud-invasion zone surrounding the borehole throughout its entire length. The presence of the mud invasion zone impacts both the pressure distribution of the surrounding formation but also increases the viscosity of the pore fluid. *In-situ* testing consisted of a 23.44 m long tool string equipped with Schlumberger's Modular Formation Dynamics Tester (MDT) tool to conduct measurements of stress magnitude, pore pressure, and permeability approximately 36 hrs after drilling had been completed. The tool was operated in two modes: single probe (SPT) and dual packer. The SPT allows the estimation of formation pressure by applying a small pancake packer to the borehole wall to isolate the formation. The dual packer test isolates an interval of 1 m to either draw down the pressure (to determine in situ pressure and permeability) or to increase fluid pressure (intended for hydraulic fracture measurements of stress magnitude). Data collected from the first two logging runs were used to select the MDT test locations, and gamma ray was included on the MDT tool to refine targeting of the measurement intervals.

2.3. MDT: Drawdown Experiment

[6] A dual packer drawdown test, in which the pressure was lowered relative to the formation pressure, was performed at 1539.2–1540.2 mbsf in an interval composed of brown-gray silty claystone with abundant siltstone-sandy siltstone interbeds. The MDT's dual packers were inflated to isolate a 1 m section where the borehole was absent of large diameter variations (in excess of 10% of the diameter) determined by inspection of the wireline caliper record. As the packers were inflated, excess pressure within the packed off zone began to develop (a sign of a good seal with the borehole wall) and this excess pressure was actively bled off by pumping fluid out of the unit into the borehole until the pressure within the zone stabilized at 39.2 MPa (Figure 2a). Borehole pressure was also monitored immediately above the packed off zone to monitor for packer seal integrity. After pressure stabilization (~80s) a drawdown test was performed by withdrawing fluid from the isolated zone at a maximum rate of 12 cm^3/s over a 130 s interval (Figure 2a). The flow rate was increased in a series of steps to the maximum rate. It was planned to draw the pressure down by 5 MPa. However, because of initial concern over borehole stability, the drawdown (black squares in Figure 2) was stopped after pressure had declined by 3.52 MPa. The beginning effective stress was 7 MPa, estimated from a minimum principal stress of 45 MPa, and in the vicinity of well bore increased to 10.48 MPa by the end of drawdown [*Saffer et al.*, 2010]). The pressure was allowed to recover for 180 s, at which point the test was terminated, again due to concerns about borehole stability. The pressure-time record shows a near linear drawdown due to the withdrawal, and a partial pressure recovery of ~0.5 MPa after pumping

was ceased. This recovery has a concave-upward form, typical of recovery tests [*Horne*, 2000]. Despite the short-duration of the test and the partial recovery of pressure, these data yields insight into formation hydraulic properties. Shipboard analysis using a curve matching technique [*Papadopulus et al.*, 1973] of the pressure recovery data yielded a permeability estimate of 1.3E-17 m^2 and a storage coefficient of 5E-11 Pa^{-1} [*Saffer et al.*, 2010]. The permeability determined using this technique is typical of silty mudstones, but the estimated storage coefficient is unreasonably low [*Gamage et al.*, 2011].

[7] To refine this estimate, we conduct 2-dimensional axial symmetric numerical models of confined fluid flow around the borehole using Comsol Multiphysics™ to simulate the complete drawdown and recovery of pressure during the test. The model domain is 100 m tall and 5000 m wide. The pumping rate is specified over a 1 m zone in the center of the model; all other boundaries were specified as no-flow. A 0.3 m radial zone around the borehole is set at the mud pressure as an initial condition due to mud invasion, whereas the region outside is set at hydrostatic pressure (based on SPT measurements of formation pressure [*Saffer et al.*, 2010]). Simulations in which this invasion zone was not incorporated failed to adequately predict the observed pressure drawdown and recovery. Fluid viscosity was fixed to a value of 2E-3 Pa-s, consistent with properties of the mud [*Saffer et al.*, 2010] because the formation surrounding the borehole was assumed to be invaded by mud. Using a the lower viscosity of the formation fluid would result in even larger permeability estimates. Permeability and storage properties of the model were iteratively modified to define a best-fit to the pressure record, as measured by the a minimum of the sum of squared residuals between observed and predicted values. The data are best fit using a permeability of 9E-17 $\pm$ 3E-17 m^2 and a storage coefficient of 8E-9 $\pm$ 4E-10 Pa^{-1} (Figure 2a). The simulated drawdown and recovery adequately captures the field data but some discrepancies are apparent, especially at early time.

2.4. MDT: Injection Experiment

[8] One goal of Expedition 319 was to obtain in-situ measurements of stress using hydraulic fracturing experiments. A hydraulic fracturing experiment was performed within a 1 m zone of the cored section at 1532.2–1533.2 mbsf. During this test the injection created significant leak-off (1400–3200 s of Figure 2b) of pressure that required an increase in injection rate to raise the pressure high enough to generate a fracture for the stress test (not shown here). The first portion of the time record (0–1400 s) in Figure 2b depicts the filling of the packer zone with fluid until the pressure begins to increase ($\sim$1400–1700 s) and the pump is stopped (at 1700 s), after which the pressure decays. After this, a series of injections raise the pressure to 41.9 MPa at $\sim$3200 s or a decreased effective stress condition of 3.1 MPa. No evidence of packer leakage was observed, suggesting that the pressure decays when pumping was stopped reflect diffusion of fluid into the formation. This presents an opportunity to estimate the permeability of the packed-off zone. Full pressure data for the test are given by *Saffer et al.* [2010] or can be accessed via http://sio7.jamstec.go.jp/expedition-index.html.

[9] Using a model identical to the one described above for the MDT-DD experiments, we simulate the injection of fluid into the formation for the hydraulic fracturing experiment. The injection rate is specified as a flux over the 1 meter zone with the same initial and boundary conditions as the model described above. Similar to the simulations above, permeability and storage properties of the model were iteratively modified to define parameters that provide a best-fit match. Because no single model captures the complexity of the observed pressure record, we report the hydraulic parameters for two simulations that bracket the observations. These models indicate a formation permeability of 1.5E-15 m^2 (Figure 2b, red line) to 5.5E-15 m^2 (Figure 2b, blue line). The best-fit storage coefficient for both simulations is 3E-7 $\pm$ 5E-8 Pa^{-1}.

2.5. Core-Based Permeability Measurements

[10] For comparison to the downhole testing results, we conducted laboratory permeability tests on 10 cm long and 5 cm in diameter silty claystone from core 4R-1, recovered at a depth of 1537.47–1537.59 mbsf. Permeability was measured parallel and perpendicular to bedding, at a confining pressure of 10 MPa and a pore pressure of 8.6 MPa. In our tests, the pore pressure is controlled at a constant value at one end of the specimen, and the other end is connected to a fixed volume reservoir. We measured permeability using the multipulse method, in which the pore pressure at the upstream sample end is increased for a fixed amount of time, then decreased, and finally increased back to its original value. Five measurements were performed in each orientation with a bedding-parallel permeability of 2.5E-19 m^2 $\pm$ 1.1E-19 m^2, and a bedding-perpendicular value of 2.7E-19 m^2 $\pm$ 5E-20 m^2. Measurements of the sample deformation during loading-unloading steps yielded a bulk modulus of $\sim$3 GPa and a storage coefficient of 1E-9 Pa^{-1}.

3. Discussion

[11] The core measurements of permeability on the claystone sample are two to four orders of magnitude lower than any of the in-situ measurements. The MDT-DD test permeability estimate (9E-17 $\pm$ 3E-17 m^2) is bracketed by the lower permeability of the core (2.5–2.7 E-19 m^2) and the higher permeability of the MDT-HF test (1.5–5.5 E-15 m^2) generating a large range of measured permeabilities, despite proximity of the two tested intervals within a relatively uniform lithologic unit (Figure 1a). The differences in permeabilities between the zones could be attributed to a variety of factors including: 1) sample support volume/scale of measurement, 2) structural or lithologic heterogeneity, and/or 3) the method/technique of measurement and analysis. Estimations of the volume of material sampled by the tests ranged from 1.5 m^3, 1.1 m^3, and 7.8 E-4 m^3 for the MDT-HF, MDT-DD, and the core sample. Volumes for the in-situ tests were determined from the size of the simulated pressure perturbation near the borehole.

[12] Porosity is a measure that is used [e.g., *Gamage et al.*, 2011] to compare sediments from different settings and at different states of consolidation (Figure 3). In sediments where hydrous minerals such as smectite clays or opal are present, intragranular porosity can lead to overestimates of porosity available for fluid flow; thus it is often corrected to account for this bound water. We use measurements of smectite content and corrected porosities for samples of the cored section at Site C0009 from *Doan et al.* [2011] to

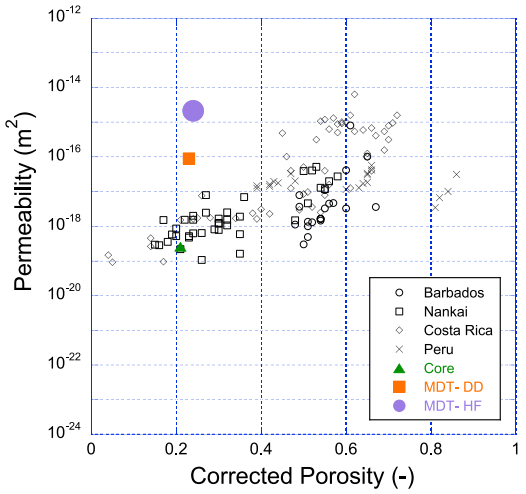

Figure 3. Plot of permeability versus corrected porosity for tests presented in this paper as well as samples from Barbados, Costa Rica, Peru, and Nankai accretionary prisms. Data in gray are from the compilation of *Gamage et al.* [2011] which are based on laboratory derived permeability estimates.

estimate the porosity of our test intervals. These corrected porosities range from 0.21–0.26.

[13] Figure 3 presents the results of this study (colored symbols Ð symbol size scaled by range of model fits), with core-based permeability-porosity relationships for a range of subduction zone mudstones (gray symbols) for comparison. The global data show a clear relationship between corrected porosity and permeability encompassing a range of permeability of roughly four orders of magnitude. Our measurements of permeability on core samples fall squarely in this range (Figure 3, green triangle). In contrast, permeability values from the MDT-DD and HF results are significantly higher than the upper envelope of core-scale measurements.

[14] Subtle lithologic heterogeneity is observed within the cored section at Site C0009, documented as cm-scale interbeds of siltystone and silty-claystone (Figure 1) although the gamma-ray log is relatively featureless. The beds are slightly thicker in core 4R (location of the MDT-DD test) compared to core 3R (location of the MDT-HF test). The larger sampling interval and support volume of the MDT-DD test would sample and bias any zones with higher permeability. It is unlikely that the permeability difference between the claystone and these thin cm-scale siltstone interbeds can explain the roughly 2-order magnitude difference in the core permeability measurement compared to the MDT-DD measurements which are within the same cored section and offset by less than 2 m in the borehole. The frequency of silty-sandstones in Core 3 and 4R averaged about 1 per meter with thicknesses on the order of 10 cm. Effective permeability layer-parallel flow calculations suggest that these 10 cm thick layers must have a permeability of at least 5E-14 m^2 (a five order of magnitude contrast to the claystones) in order to explain the MDT-HF and MDT-DD results. Considering the grain-size, sorting, and consolidation state of these thin interbeds and compared to other subduction zone materials at similar porosities (gray symbols in Figure 3), it is unlikely that these interbeds can explain the high permeabilities of the tests.

[15] Both the MDT-DD and MDT-HF were located in the cored section of the borehole where detailed structural analysis revealed both open and annealed fractures (i.e., faults and shear zones, respectively). Both structures have generally similar densities per meter. The faults, however, because they are younger and appeared as open fractures in the opened core barrel probably have the greatest potential as conduits for fluid flow. Considering a linear fracture intensity of 3.4 per meter for the faults and attributing all flow to the fractures and applicability of the cubic law, calculations suggest an average apertures of 7 and 26 μm for fractures in the MDT-DD and MDT-HF testing zones. Inspection of the FMI logs at the MDT testing depths also indicates open fractures. We therefore contend that the larger testing intervals of the MDT experiments sampled the faults observed in the core, and that this explains their high permeabilities relative to values from core-scale laboratory measurements. The even higher permeability estimated from the MDT-HF test could be the result of multiple fractures of different dips intersecting the borehole leading to a more connected and higher permeability backbone of the fracture network. Another plausible explanation could be that since the injection pressure was higher than the formation pressure it caused a decrease in effective stress allowing fractures to dilate and increasing the permeability, which could also explain the increasing mid-fit of the MDT-HF with time (or effective stress decrease). This stress sensitivity of fractures has been observed in a variety of tectonic environments [*Barton et al.*, 1995].

4. Conclusions

[16] In-situ measurements of permeability were undertaken during a recent IODP expedition (NanTroSEIZE experiment). Two in-situ measurements of permeability with the MDT tool sample large volume of material and yield permeability estimates that are orders of magnitude larger than core-based measurements of permeability for materials from the same section of the borehole. Additionally, these permeability estimates obtained from numerical modeling range from 5 E-15–9E-17 m^2, are significantly higher than permeability measurements on core samples of similar porosity from other subduction zones. Natural fractures, both open and sealed, were prevalent in this interval and we conclude that they could be responsible for increasing the permeability beyond the low matrix permeability of the clay-dominated sediments. The occurrence of fracture permeability in these settings has not been previously mentioned or observed and has implications for the permeability structure of deformed accretionary prisms as well as the resulting ability to drain excess pore pressure from consolidation or deformation. Research into permeability of fractured and deformed wedge material afforded by upcoming drilling expeditions should yield additional insight into fracture permeability. Considerations of sampling and testing fractured material, as opposed to intact and undisturbed samples, for core-based experiments could remove some of the bias between *in-situ* and laboratory measurements.

[17] **Acknowledgments.** This research used samples and/or data provided by the Integrated Ocean Drilling Program (IODP). Funding for this research was provided by a U.S. Science Support Program Post-Expedition award to Boutt.

[18] The Editor thanks Brandon Dugan and an anonymous reviewer for their assistance in evaluating this paper.

References

Barton, C. A., M. Zoback, and D. Moos (1995), Fluid flow along potentially active faults in crystalline rock, *Geology*, *23*, 683–686.

Becker, K., and E. Davis (2004), *In Situ Determinations of the Permeability of the Igneous Oceanic Crust*, pp. 189–224, Cambridge Univ. Press, Cambridge, U. K.

Bekins, B. A., A. McCaffrey, and S. Dreiss (1995), Episodic and constant flow models for the origin of low-chloride waters in a modern accretionary complex, *Water Resour. Res.*, *31*, 3205–3215.

Bekins, B. A., D. Matmon, E. Screaton, and K. Brown (2011), Reanalysis of *in situ* permeability measurements in the Barbados decollement, *Geofluids*, *11*(1), 57–70.

Brown, K. (1995), The variation of the hydraulic conductivity structure of an overpressured thrust zone with effective stress, *Proc. Ocean Drill. Progam Sci. Results*, *146*, 281–289.

Bruckmann, W., K. Moran, and A. Mackillop (1997), Permeability and consolidation characteristics from Hole 948B, northern Barbados Ridge, *Proc. Ocean Drill. Progam Sci. Results*, *156*, 109–114.

Davis, D., J. Suppe, and F. Dahlen (1983), Mechanics of fold-and-thrust belts and accretionary wedges, *J. Geophys. Res.*, *88*, 1153–1172.

Davis, E., and K. Becker (2002), Observations of natural-state fluid pressures and temperatures in young oceanic crust and inferences regarding hydrothermal irculation, *Earth Planet. Sci. Lett.*, *204*(1–2), 231–248.

Davis, E. E., K. Wang, K. Becker, and R. E. Thomson (2000), Formation-scale hydraulic and mechanical properties of oceanic crust inferred from pore pressure response to periodic seafloor loading, *J. Geophys. Res.*, *105*, 13,423–13,435.

Doan, M.-L., M. Conin, P. Henry, T. Wiersberg, D. Boutt, D. Buchs, D. Saffer, L. C. McNeill, D. Cukur, and W. Lin (2011), Quantification of free gas in the Kumano fore-arc basin detected from borehole physical properties: IODP NanTroSEIZE drilling Site C0009, *Geochem. Geophys. Geosyst.*, *12*, Q0AD06, doi:10.1029/2010GC003284.

Fisher, A. (2005), Marine hydrogeology: Recent accomplishments and future opportunities, *Hydrogeol. J.*, *13*, 69–97.

Fisher, A., and G. Zwart (1996), Relation between permeability and effective stress along a plate boundary fault, Barbados accretionary complex, *Geology*, *24*, 307–310.

Gamage, K., and E. Screaton (2006), Characterization of excess pore pressures at the toe of the Nankai accretionary complex, Ocean Drilling Program sites 1173, 1174, and 808: Results of one-dimensional modeling, *J. Geophys. Res.*, *111*, B04103, doi:10.1029/2004JB003572.

Gamage, K., E. Screaton, B. A. Bekins, and I. Aiello (2011), Permebility-porosity relationships of subduction zone sediments, *Mar. Geol.*, *279*(1–4), 19–36.

Horne, R. N. (2000), *Modern Well Test Analysis*, Petroway, Palo Alto, Calif.

Hsieh, P. A. (1998), Scale dependence and scale invariance in hydrology, in *Rock Mechanics as a Multidisciplinary Science*, pp. 335–353, Cambridge Univ. Press, New York.

Matmon, D., and B. A. Bekins (2006), Hydromechanics of a high taper angle, low-permeability prism: A case study from Peru, *J. Geophys. Res.*, *111*, B07101, doi:10.1029/2005JB003697.

Papadopulos, S. S., J. D. Bredehoeft, and H. H. Cooper Jr. (1973), On the analysis of 'slug test' data, *Water Resour. Res.*, *9*, 1087–1089.

Saffer, D. M., and B. A. Bekins (1998), Episodic fluid flow in the Nankai accretionary complex: Timescale, geochemistry, flow rates, and fluid budget, *J. Geophys. Res.*, *103*, 30,351–30,370.

Saffer, D. M., and B. A. Bekins (2002), Hydrologic controls on the morphology and mechanics of accretionary wedges, *Geology*, *30*, 271–274.

Saffer, D., et al. (2010), *NanTroSEIZE Stage 2: Riser/Riserless Observatory*, *Proc. Integr. Ocean Drill. Program*, 319.

Scholz, C. (1998), Earthquakes and friction laws, *Nature*, *391*, 37–42.

D. F. Boutt, Department of Geosciences, University of Massachusetts-Amherst, 611 N. Pleasant St., 233 Morrill Science Cent., Amherst, MA 01003, USA. (dboutt@geo.umass.edu)

T. Byrne, Center for Integrative Geosciences, University of Connecticut, U-45 354 Mansfield Rd., Storrs, CT 06269, USA.

M.-L. Doan, ISTerre, Université Joseph Fourier, BP53, 1381, rue de la Piscine, F-38041 Grenoble CEDEX, France.

P. Flemings, Jackson School of Geosciences, University of Texas at Austin, 1 University Stn. C1100, Austin, TX 78712, USA.

N. W. Hayman, Institute for Geophysics, University of Texas at Austin, PRC 196, 10100 Burnet Rd., Austin, TX 78758, USA.

T. Ito, Institute of Fluid Science, Tohoku University, 2-1-1 Katahira, Aoba-ku, Sendai, Miyagi 980-8577, Japan.

Y. Kano, Disaster Prevention Research Institute, Kyoto University, Gokasho, Uji, Kyoto 611-0011, Japan.

W. Lin, Kochi Institute for Core Sample Research, JAMSTEC, 200 Monobe-otsu, Nankoku, Kochi 783-8502, Japan.

L. C. McNeil, Southampton Oceanography Centre, University of Southampton, Southampton SO14 3ZH, UK.

K. T. Moe, Center for Deep Earth Exploration, JAMSTEC, 3173-25 Showa-machi, Kanazawa-ku, Yokohama, Kanagawa 236-0001, Japan.

D. Saffer, Department of Geosciences, Pennsylvania State University, University Park, PA 16802, USA.